繰り返し誘導遷移を利用した超解像非線形蛍光顕微鏡

嶽　文宏*，林　世莉*

Super-resolution nonlinear fluorescence microscopy using repetitive stimulated transition

Fumihiro DAKE* and Seri HAYASHI*

光の回折限界を超えた超解像蛍光顕微鏡はバイオイメージングにおいて不可欠なツールとなっている．種々の手法が提案実証されており，その多くが光と物質の相互作用を効果的に活用している．我々は，繰り返し誘導遷移 (REST, Repetitive stimulated transition) という物理現象を提起し，これを利用した超解像非線形蛍光顕微鏡を提案実証している．REST 顕微鏡では，２色のレーザー光が誘起する誘導吸収（励起）と誘導放出を複数回経て生じる非線形蛍光をロックイン検出することで画像を取得する．非線形蛍光の信号発生領域が入射光の点像強度分布関数の多重積となるため，超解像効果が得られる．蛍光ビーズ・生物試料イメージングの結果は，提案手法による分解能向上効果を明瞭に示している．本稿では REST 顕微鏡について総説する．まず始めに，蛍光と非線形蛍光に関する現象論的モデルを用いて，REST の種類と特長について述べる．次に，これまでの REST 顕微鏡の原理確認実験結果について紹介する．最後に，非線形蛍光の考察と今後の展望について述べる．

In developing super-resolution fluorescence microscopy, light–matter interactions allow the diffraction barrier to be broken. Super-resolution nonlinear fluorescence microscopy is presented in this study using a unique light–matter interaction named as repetitive stimulated transition (REST), caused by two-color laser beams. The resulting nonlinear fluorescence, which undergoes the aforementioned REST processes, is detectable as a signal via the lock-in technique. The signal is produced by the multiplicative combination of incident beams leading to an improvement of the three-dimensional optical resolution. Imaging results of fluorescent beads indicate that REST microscopy has a superior optical resolution compared to conventional laser-scanning fluorescence microscopy. Biological imaging results verify the acceptable feasibility of REST microscopy for practical use. In this review article, the phenomenological model to describe the mechanisms and characteristics of REST processes is presented. Then, the recent advancement of REST microscopy using two distinctive REST processes implemented with pulsed and continuous-wave lasers respectively, is described. Finally, a general outlook of nonlinear fluorescence microscopy is given.

Key words 蛍光顕微鏡，非線形顕微鏡，超解像，誘導吸収，誘導放出
fluorescence microscopy, nonlinear microscopy, super-resolution, stimulated absorption, stimulated emission

1 Introduction

Fluorescence microscopy is an indispensable tool in the field of biology and is widely used for a variety of biological imaging applications[1]. However, the optical resolution remains limited to about half of the wavelength on account of the diffraction limit[2]. To surpass the diffraction barrier, several super-resolution techniques utilizing the nonlinearity of various light–matter interactions have been applied[3)~12)].

Recently, super-resolving nonlinear fluorescence (NF) microscopy that employs repetitive stimulated transition (REST) processes caused by two-color laser beams[13)14)] was proposed. The NF is produced by the multiplicative combination of both incident beams, resulting in the improvement of the three-dimensional optical resolution — theoretically to an unlimited extent. There are two REST processes, their main difference being the origin of the saturation effect[13)14)]. Both methods are similar, but have different physical phenomena leading to offbeat signal properties, such as optical resolution, quantum-limited sensitivity, and tolerance to photodamage.

In this review article, first the phenomenological model to

* 研究開発本部　光技術研究所

describe the mechanisms and characteristics of NF including REST processes is presented. Then, the recent advancement of REST microscopy using different REST processes implemented with pulsed and continuous-wave (CW) lasers respectively, is described. Finally, a general outlook over NF microscopy is given.

2 Phenomenological interpretation of REST processes

Figure 1 describes the phenomenological interpretation for linear fluorescence (LF) and NF. The wavelengths of the pump and probe beams overlap the absorption and emission spectra of the fluorescent dye, respectively. Thus the pump beam induces stimulated absorption (SA) and the probe beam induces stimulated emission (SE). In the LF process (Fig. 1(a)), the pump beam induces SA (i.e., excitation), then generates fluorescence. In the lowest NF (LNF) process (Fig. 1(b)), the pump beam excites fluorophores, a few of which are reverted to the ground state by SE from the probe beam. The NF signal is then produced. The detectable NF wavelength is different from the probe wavelength. The LNF microscopy was previously implemented with pulsed lasers[6)7)] and CW lasers[8)15)]. In REST processes (Figs. 1(c) and (d)), a few fluorophores, which were excited by the pump beam and then reverted by the probe beam, are excited again by the pump or probe beam, resulting in the production of higher-order NF signals (i.e., REST signals). These re-excitations are due to the finite lifetime of the high vibrational state within the ground state, after fluorophores are reverted by SE[16)]. This is generally considered to have a negative effect on Stimulated emission depletion (STED) microscopy since the re-excitation unavoidably disturbs complete fluorescence quenching. Contrastingly, REST microscopy can utilize these re-excitations as the origin of signal production. It appears that REST processes are higher-order nonlinear phenomena compared to the LNF process. REST processes can be interpreted as a part of a saturation effect[13)]. The REST process based on the re-excitation caused by the pump beam (Fig. 1(c)) can be interpreted as the saturation effect of SA. On the other hand, the REST process based on the re-excitation caused by the probe beam (Fig. 1(d)) can be interpreted as the saturation effect of SE.

Optical resolutions for the LF and NF processes can be roughly estimated from the phenomenological model. For simplicity, it is assumed that the optical resolution is determined solely by the incident beam, ignoring the pinhole effect[17)]. The LF signal is proportional to the pump beam; therefore, its resolution is determined by the pump point spread function (PSF). The LNF signal is proportional to the product of the pump and probe beams; therefore, its resolution is determined by the product of both beam PSFs, resulting in a superior resolution to the LF signal[6)~8)]. In a similar manner, REST signals are proportional to the product of the three beams; therefore, optical resolutions are determined by the product of the three PSFs, resulting in superior resolutions compared to the LF and the LNF signals. The theoretical expectation can be estimated using a resolution scaling factor of $1/\sqrt{i}$ [13)], where i is the number of associated stimulated transitions. The specific theoretical formulas for both REST processes are described in our previous works[13)14)].

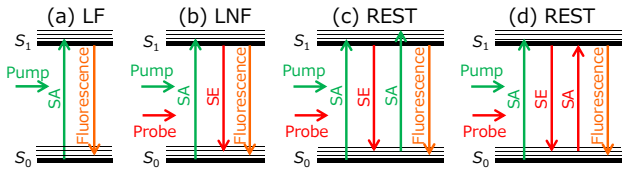

Fig. 1 Phenomenological interpretation for LF and NF processes: (a) LF, (b) LNF, (c) and (d) REST caused by the saturation effects of SA and SE, respectively. S_0: population of the ground state, S_1: population of the excited state.

To extract the REST signal from the total fluorescence signal practically, it is necessary to use a lock-in technique. The intensities of the pump and probe beams should be modulated with sinusoidal waves at frequencies of f_1 and f_2, respectively. The REST signal can be detected with a demodulation frequency of $mf_1 \pm nf_2$ [13)], where m and n are the numbers of associated stimulated transitions caused by the pump and probe beams, respectively ($m + n = i$).

3 Experimental setup

Figure 2 shows the experimental setup for REST microscopy, the details are described in our previous works[13)14)]. Two-color lasers are used for the pump and probe beams. The pump wavelength is set within the absorption spectrum of the fluorescent dyes. The probe wavelength is set within the red tail of the emission maximum. Pulsed and CW lasers are used for the proof-of-concept demonstration of REST processes based on the saturation of SA (Fig. 1(c)) and SE (Fig. 1(d)), respectively. The intensities of the pump and probe beams are temporally modulated by acousto-optic modulators with sinusoidal waves at modulation frequencies of f_1 = 2 MHz and f_2 = 2.7 MHz. Then, both beams are focused into a sample via an objective lens (Nikon, CFI Plan Apo VC 100X/1.4 Oil) that induces the light-matter interac-

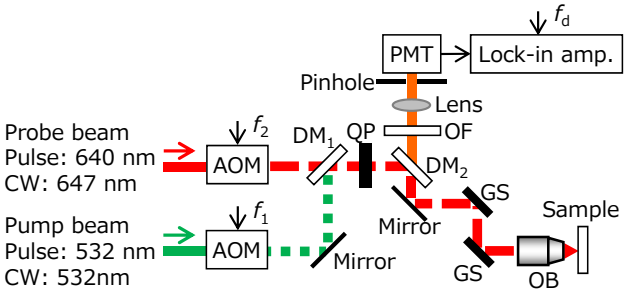

Fig. 2 Experimental setup for REST microscopy. AOM: acousto-optic modulator, DM: dichroic mirror, QP: quarter-wave plate, GS: galvano scanner, OB: objective lens, OF: optical filter, PMT: photomultiplier tube. f_d: demodulation frequency.

tions such as: LF, LNF and REST processes. A backscattering fluorescence is passed through an optical filter (593 ± 23 nm), which removes both pump and probe beams. Fluorescence is focused into a pinhole with a diameter of 30 μm (~1 airy) and detected with a photomultiplier. The detector photocurrent is then determined by a lock-in amplifier.

4 Demonstration of REST microscopy using the saturation of SA implemented with pulsed lasers

The REST process based on the saturation of SA was applied with two-color picosecond pulsed lasers[13]. Figure 3 shows the experimental results for REST signal detection. A fluorescent solution consisting of ATTO 550 dissolved in water at a concentration of approximately 1 μg/μL was employed as a test sample. Figure 3(a) shows the dependence of the lock-in signals on the pump optical power. The LF signal was detected with a demodulation frequency of f_1, when employing only the pump beam. The REST signal was detected with a demodulation frequency of $2f_1 - f_2$ (1.3 MHz), when employing both the pump and probe beams. The results confirmed that the LF signal was proportional to the 0.9^{th} power of the pump power, in good agreement with the pump power dependence of LF. On the other hand, the results also confirmed that the REST signal was proportional to the 2.1^{th} power of the pump power. This result is also in good agreement with the pump power dependence of the REST process. Figure 3(b) shows the dependence of the lock-in signal on the probe optical power. The REST signal was proportional to the 0.9^{th} power of the probe power. This result was in good agreement with the probe power dependence of the REST process. Therefore, these results confirm that the lock-in signals demodulated with $2f_1 - f_2$ originate from the REST process based on the saturation of SA (Fig. 1(c)).

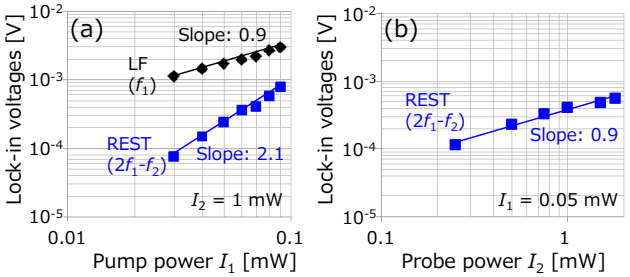

Fig. 3 Experimental results for REST signal detection[13]. (a) Lock-in signals as a function of the pump power. (b) Lock-in signals as a function of the probe power.

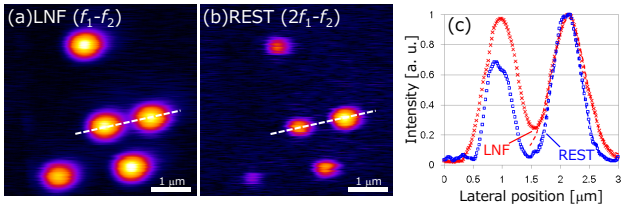

Fig. 4 Imaging results of fluorescent beads with a diameter of 500 nm[13]. (a) LNF and (b) REST images. I_1 = 0.1 mW, I_2 = 1.5 mW. Image acquisition time: 5 s. (c) Line profiles along the white dashed lines indicated in (a, b).

Figure 4 shows the imaging results of fluorescent beads with a diameter of 500 nm. Figures 4(a) and (b) show LNF and REST images, respectively. The LNF and REST signals were detected with demodulation frequencies of $f_1 - f_2$ (0.7 MHz) and $2f_1 - f_2$ (1.3 MHz), respectively. The imaging results showed that the bead diameter in the REST image was narrower than in the LNF image. Figure 4(c) shows line profiles of the images. The intensity of the REST signal between the two beads sharply declined, indicating that the REST signal has a higher resolution than the LNF signal. The full-width at half-maximum (FWHMs) of the bead profiles captured by LNF and REST were 684 nm and 539 nm, respectively. Since the bead diameter was larger than the diffraction-limited resolution, the estimated FWHMs do not directly provide optical resolution. Nevertheless, the experimental results clearly demonstrate the scalability of optical resolution and provide sufficient evidence of resolution improvement using the REST process.

5 Demonstration of REST microscopy using the saturation of SE implemented with CW lasers

The REST process based on the saturation of SE was

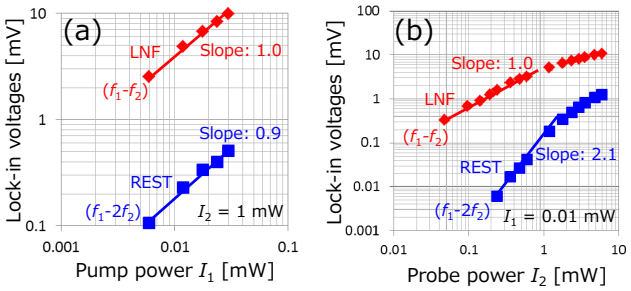

Fig. 5 Experimental results of REST signal detection[14]. (a) Lock-in signals as a function of the pump power. (b) Lock-in signals as a function of the probe power.

applied with two-color CW lasers[14]. Figure 5 shows the experimental results for REST signal detection. A fluorescent solution (ATTO 550) was used as a sample. LNF and REST signals were detected with demodulation frequencies of $f_1 - f_2$ (0.7 MHz) and $f_1 - 2f_2$ (3.4 MHz), respectively. Figure 5(a) shows the dependence of the lock-in signals on the pump optical power. The LNF and REST signals were proportional to the 1.0^{th} and 0.9^{th} powers of the pump power, respectively. These results were in good agreement with the pump power dependence of the LNF and REST signals. Figure 5(b) shows the dependence of the lock-in signals on the probe optical power. The LNF signal was proportional to the 1.0^{th} power of the probe power. On the other hand, the REST signal was proportional to the 2.1^{th} power of the probe power. Both power properties were in good agreement with the probe power dependence of the LNF and REST signals, respectively. These results are effective evidence that the lock-in signal demodulated with $f_1 - 2f_2$ originates from the REST process based on the saturation of SE (Fig. 1(d)). Under these experimental conditions, the REST signal did not follow the square-root law when the probe power reached several milliwatts (Fig. 5(b)). The saturation of a certain NF signal indicates the generation of higher-order NF signals[4]. It should be noted that the REST signal saturation gives rise to an unavoidable negative effect that worsens the optical resolution, since it three-dimensionally expands the signal generation volume. In this case, it is desirable to detect a higher-order REST signal that can be detected with a demodulation frequency of $f_1 - nf_2$ ($n > 2$).

Figure 6 shows the imaging results of fluorescent beads with a diameter of 200 nm. Figures 6(a) and (b) show the LNF and REST images, respectively. Figure 6(c) shows line profiles of both images. The FWHMs of the bead profiles acquired by the LNF and REST signals were 289 nm and 251 nm, respectively. Because the bead diameter is smaller than the diffraction-limited resolution, the estimated FWHMs become approximately equal to their respective optical resolutions. These results demonstrate that the REST signal has a 1.2 times higher lateral resolution than the LNF signal. Figure 6(d) shows axial line profiles of the fluorescent beads. The FWHMs of the bead profiles acquired by the LNF and REST signals were 913 nm and 721 nm, respectively. Therefore, the REST signal has a 1.3 times higher axial resolution than the LNF signal. The theoretical value can be estimated by the resolution scaling factor of $1/\sqrt{i}$ [13]. The theoretical FWHM ratio of LNF ($i = 2$) to REST ($i = 3$) is calculated as $\sqrt{(3/2)} = 1.22$. Therefore, it was confirmed that the experimental result was in good agreement with the theoretical expectation.

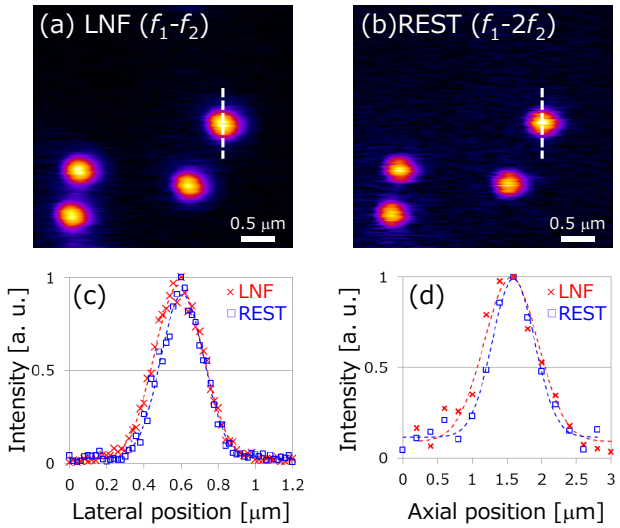

Fig. 6 Imaging results of fluorescent beads with a diameter of 200 nm[14]. (a) LNF and (b) REST images. (c) Line profiles along the white dashed lines indicated in (a) and (b). (d) Axial line profiles of the fluorescent beads. Image acquisition time: 1 s. I_1 = 12 μW, I_2 = 2 mW.

Figure 7 shows the imaging results of the spheroid sample, where the actin of HT-29 cells was labeled with ATTO 550 dye. Images were captured via a water immersion objective lens (Nikon, CFI Plan Apo VC 60XC/1.2 WI). Figure 7(a) shows the confocal fluorescence (CF) image captured with a demodulation frequency of f_1 while employing solely the pump beam. Figure 7(b) shows the REST image. Figure 7(c) shows line profiles of the images. These results demonstrate that the REST image has a better optical resolution and contrast than the CF image. Imaging results also reveal that even REST microscopy implemented with CW lasers can be sufficient for biological application. Thus, the feasibility of REST microscopy for practical use was verified.

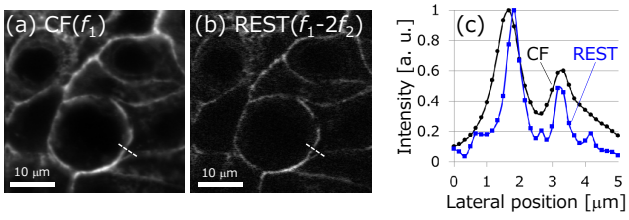

Fig. 7 Imaging results of the spheroid sample[14]. (a) CF and (b) REST images. (c) Line profiles along the white dashed lines in (a) and (b). Imaging depth: 10 μm. Image acquisition time: 1 s. I_1 = 40 μW, I_2 = 4 mW.

6 Discussion and Outlook

Both distinctive REST processes (Figs. 1(c) and (d)) caused by the saturation of SA and SE have complementary features. The optical resolution of the former REST signal is superior to that of the latter because of the difference between the pump and probe wavelengths ($\lambda_1 < \lambda_2$). The photodamage caused by the probe beam is potentially less problematic than that caused by the pump beam because the probe beam is intrinsically transparent to the sample. In terms of quantum limit sensitivity, the latter REST signal ($\propto I_1 I_2^2$) is potentially less susceptible to shot noise than the former REST signal ($\propto I_1^2 I_2$). An increase of the pump intensity boosts the LF signal, resulting in a definite increase of the shot noise. On the other hand, the probe beam does not produce the LF signal; an increase of the probe intensity decreases the fluorescence photons due to SE, resulting in a reduction of the shot noise.

Both pulsed and CW lasers were used as light sources for REST microscopy. It is apparent that pulsed lasers are more efficient in generating NF signals than CW lasers. However, the need for a pulsed laser inevitably disturbs the wider use of this method due to the high cost, low robustness, and narrow wavelength selectivity. CW lasers enable REST microscopy in a more practical way. In STED microscopy, equivalent fluorescence quenching can be achieved by both types of lasers — as long as the CW laser power reaches several folds compared to the averaged power of the pulsed laser[18]. Thereby, it is expected that the REST image qualities captured by CW and pulsed lasers could be identical. Judging from the fact that photobleaching occurs predominantly from the laser peak intensity[19], CW lasers are potentially less harmful than pulsed lasers. The image acquisition time is virtually irrelevant to the laser type because it is predominantly determined by the lock-in frequencies.

The present optical setup enables both REST signals to be acquired, as well as the conventional LF and LNF signals, via the appropriate setting of the demodulation frequency. It is desirable to select appropriate NF signals based on the imaging and sample conditions. It should be noted that NF signals can intrinsically retain their sectioning ability without the pinhole due to the nonlinearity[6)20)], while the LF signal cannot retain this without the pinhole. The pinhole effect theoretically extends the frequency cutoff in both LF and NF microscopy, and a smaller pinhole is desirable[17]. However, too small of a pinhole is problematic for photon detection efficiency in thick sample imaging due to the light deflection or scattering impacts. It is advisable to set an appropriate pinhole size which can achieve balance between image quality and optical resolution.

Fluorescence lifetime imaging (FLIM) is a promising application for NF microscopy. Fluorescence lifetime enables fluorophores with the same emission spectrums, but different lifetimes, to be distinguished and therefore improve the molecular discrimination capacity[21)22)]. Fluorescence lifetime essentially depends on the molecular conformation and the manner in which the molecule interacts with its environment; therefore, FLIM can elucidate molecular interactions and dynamics[23)~26)]. The LNF signal has previously been applicable to FLIM[6)7)27)]. The REST signal is also expected to be applicable for FLIM with a higher optical resolution than the LNF signal, which enables visualization of biological interactions on a subcellular scale. Such versatility will be useful for a variety of sample observations.

7 Summary

In this review article, first the mechanisms and characteristics of REST processes with phenomenological interpretation were presented. Then, the application of REST microscopy using saturation effects of SA and SE implemented with pulsed and CW lasers respectively, was described. Finally, a general outlook over NF including REST processes was given. REST microscopy is pursued in order to make it a beneficial approach for the visualization of various biological interactions and dynamics on a subcellular scale.

Acknowledgment. The authors are grateful to Y. Taki, N. Fukutake, and Y. Fujikake of Nikon Corporation for the fruitful discussions and insights.

References

1) B. N. G. Giepmans, S. R. Adams, M. H. Ellisman and R. Y. Tsien: *Science*, **312** (2006) 217.
2) J. B. Pawley: *Handbook of Biological Confocal Microscopy* (Springer Science + Business Media, 2006).

3) B. Hein, K. I. Willig and S. W. Hell: *Pro. Natl. Acad. Sci. USA*, **105** (2008) 14271.
4) K. Fujita, M. Kobayashi, S. Kawano, M. Yamanaka and S. Kawata: *Phys. Rev. Lett.*, **99** (2007) 228105.
5) K. Isobe, A. Suda, H. Hashimoto, F. Kannari, H. Kawano, H. Mizuno, A. Miyawaki and K. Midorikawa: *Biomed. Opt. Express*, **1** (2010) 791.
6) C. Y. Dong, P. T. C. So, T. French and E. Gratton: *Biophys. J.*, **69** (1995) 2234.
7) F. Dake and Y. Taki: *Appl. Opt.*, **57** (2018) 757.
8) J. Miyazaki, H. Tsurui, A. Hayashi-Takagi, H. Kasai and T. Kobayashi: *Opt. Express*, **22** (2014) 9024.
9) M. G. L. Gustafsson: *Proc. Natl. Acad. Sci. USA*, **102** (2005) 13081.
10) E. H. Rego, L. Shao, J. J. Macklin, L. Winoto, G. A. Johansson, N. K. Hughes, M. W. Davidson and M. G. L. Gustafsson: *Proc. Natl. Acad. Sci. USA*, **109** (2012) E135.
11) F. Dake, S. Nakayama and Y. Taki: *Opt. Rev.*, **22** (2015) 598.
12) F. Dake: *Opt. Rev.*, **23** (2016) 587.
13) F. Dake, N. Fukutake, S. Hayashi and Y. Taki: *Appl. Phys. Express*, **11** (2018) 012401.
14) F. Dake and S. Hayashi: *Opt. Lett.*, **44** (2019) 3402.
15) C. Y. Dong, C. Buehler, P. T. C. So, T. French and E. Gratton: *Appl. Opt.*, **40** (2001) 1109.
16) M. Leutenegger, C. Eggeling and S. W. Hell: *Opt. Express*, **18** (2010) 26417.
17) C. Y. Dong, P. T. C. So, C. Buehler and E. Gratton: *Optik*, **106** (1997) 7.
18) K. I. Willig, B. Harke, R. Medda and S. W. Hell: *Nat. Methods*, **4** (2007) 915.
19) M. Dyba and S. W. Hell: *Appl. Opt.*, **42** (2003) 5123.
20) L. V. Doronina-Amitonova, I. V. Fedotov and A. M. Zheltikov: *Opt. Lett.*, **40** (2015) 725.
21) K. Carlsson and A. Liljeborg: *J. Microscopy*, **185** (1997) 37.
22) J. Bückers, D. Wildanger, G. Vicidomini, L. Kastrup and S. W. Hell: *Opt. Express*, **19** (2011) 3130.
23) M. K. Kuimova, G. Yahioglu, J. A. Levitt and K. Suhling: *J. Am. Chem. Soc.*, **130** (2008) 6672.
24) J. R. Lakowicz, H. Szmacinski, K. Nowaczyk and M. L. Johnson: *Proc. Natl. Acad. Sci. USA*, **89** (1992) 1271.
25) S. Ogikubo, T. Nakabayashi, T. Adachi, M. S. Islam, T. Yoshizawa, M. Kinjo and N. Ohta: *J. Phys. Chem. B*, **115** (2011).
26) D. Li, W. Zheng and J. Y. Qu: *Opt. Lett.*, **33** (2008) 2365.
27) J. Miyazaki, K. Kawasumi and T. Kobayashi: *Rev. Sci. Instrum.*, **85** (2014) 093703.